Cardiovascular Research (2012) **95**, 308–316
doi:10.1093/cvr/cvs183

Role of the transient outward potassium current in the genesis of early afterdepolarizations in cardiac cells

Zhenghang Zhao[1,2†], Yuanfang Xie[3†], Hairuo Wen[2], Dandan Xiao[1], Charelle Allen[2], Nadezhda Fefelova[2], Wen Dun[4], Penelope A. Boyden[4], Zhilin Qu[3*], and Lai-Hua Xie[2*]

[1]Department of Pharmacology, School of Medicine, Xi'an Jiaotong University, Xi'an, China; [2]Department of Cell Biology and Molecular Medicine, UMDNJ-New Jersey Medical School, MSB G609, Newark, NJ 07103, USA; [3]Department of Medicine (Cardiology), David Geffen School of Medicine at UCLA, A2-237 CHS, 650 Charles E. Young Drive South, Los Angeles, CA 90095, USA; and [4]Department of Pharmacology, Columbia University, New York, NY, USA

Received 19 March 2012; revised 10 May 2012; accepted 29 May 2012; online publish-ahead-of-print 1 June 2012

Time for primary review: 21 days

Aims The transient outward potassium current (I_{to}) plays important roles in action potential (AP) morphology and dynamics; however, its role in the genesis of early afterdepolarizations (EADs) is not well understood. We aimed to study the effects and mechanisms of I_{to} on EAD genesis in cardiac cells using combined experimental and computational approaches.

Methods and results We first carried out patch-clamp experiments in isolated rabbit ventricular myocytes exposed to H_2O_2 (0.2 or 1 mM), in which EADs were induced at a slow pacing rate. EADs were eliminated by either increasing the pacing rate or blocking I_{to} with 2 mM 4-aminopyridine. In addition to enhancing the L-type calcium current ($I_{Ca,L}$) and the late sodium current, H_2O_2 also increased the conductance, slowed inactivation, and accelerated recovery from the inactivation of I_{to}. Computer simulations showed that I_{to} promoted EADs under the condition of reduced repolarization reserve, consistent with the experimental observations. However, EADs were only promoted in the intermediate ranges of the I_{to} conductance and the inactivation time constant. The underlying mechanism is that I_{to} lowers the AP plateau voltage into the range at which the time-dependent potassium current (namely I_{Ks}) activation is further slowed and $I_{Ca,L}$ is available for reactivation, leading to voltage oscillations to manifest EADs. Further experimental studies in cardiac cells of other species validated the theoretical predictions.

Conclusion In cardiac cells, I_{to}, with a proper conductance and inactivation speed, potentiates EADs by setting the AP plateau into the voltage range where $I_{Ca,L}$ reactivation is facilitated and I_{Ks} activation is slowed.

Keywords Transient outward current • Early afterdepolarization • Cardiac arrhythmias • Computer model • Dynamic mechanisms

1. Introduction

The transient outward potassium (K) current (I_{to}) has been shown to play important roles in the action potential (AP) morphology and AP duration (APD) alternans,[1–3] which has been linked to arrhythmogenesis in Brugada syndrome.[4] In a study by Guo *et al.*,[5] it was shown that the elimination of I_{to} in mouse ventricular myocytes increased the propensity of early afterdepolarizations (EADs). EADs are secondary depolarizations or oscillations during the AP plateau or repolarizing phase, which are associated with arrhythmogenesis in cardiac diseases, such as long QT syndrome.[6,7] It is well accepted that EADs are facilitated under conditions of reduced repolarization reserve,[8,9] in which APDs are prolonged by either increasing inward currents or decreasing outward currents, or both. It should be noted that although a reduced repolarization reserve prolongs the APD, simply lengthening the APD does not necessarily lead to EADs. In a recent theoretical study,[10] Tran *et al.* showed that in addition to a reduced repolarization reserve, the activation and inactivation kinetics of $I_{Ca,L}$ must be

† These authors contributed equally to this work.

* Corresponding author. Tel: +1 973 972 2411 (L.-H.X.)/+1 310 794 6050 (Z.Q.); fax: +1 973 972 7489 (L.-H.X.)/+1 310 206 9133 (Z.Q.), Email: xiela@umdnj.edu (L.-H.X.)/zqu@mednet.ucla.edu (Z.Q.)

properly matched to cause the voltage oscillations underlying EADs. In addition, the activation time of the slow time-dependent K current (namely I_{Ks}) must be slow enough to allow the voltage oscillations to manifest during the plateau or repolarizing phase. More specifically, the membrane voltage must decline to <0 mV quickly enough before I_{Ks} has sufficient time to fully activate so that $I_{Ca,L}$ can be reactivated while the repolarization reserve is still low. This leads us to hypothesize that I_{to}, by lowering the AP plateau voltage into the range at which I_{Ks} activation is slowed and $I_{Ca,L}$ is available for reactivation, can lead to voltage oscillations to manifest EADs. In our previous study,[11] we showed that exogenous addition of H_2O_2 to myocytes induces EADs, which is probably mediated by the activation of Ca/calmodulin kinase II (CaMK II),[12] and the consequent activation of the L-type calcium current ($I_{Ca,L}$) and the late sodium current (I_{Na}).[13–16] In the present study, we used this H_2O_2-induced EAD model and confirmed our hypothesis via experimental and theoretical studies.

2. Methods

2.1 Patch-clamp experiments

This investigation conforms with the *Guide for the Care and Use of Laboratory Animals*, published by the National Institutes of Health (NIH Publication No. 85–23, Revised 1996). All animal experimental procedures were reviewed and approved by the Institutional Animal Care and Use Committee at the University of Medicine and Dentistry of New Jersey-New Jersey Medical School, by the Ethical Committee of Xi'an Jiaotong University, and by the Institutional Animal Care and Use Committee at Columbia University.

2.1.1 Single cell isolation

Myocytes were enzymatically isolated from the left ventricles of adult rabbit, rat, and mouse hearts in Langendorff fashion at 37°C with collagenase and protease.[11,17] Canine epicardial ventricular myocytes were isolated from the LV sections. Canine Purkinje cells were isolated from the Purkinje fibres of both right and left ventricles. The animals were euthanized with Euthasol (0.22 mL/kg, i.e. pentobarbital 86 mg/kg + phenytoin 11 mg/kg; iv in rabbits and ip in rats and mice) or anaesthetized with propofol (5–15 mg/kg; iv in dogs). Immediately after the cessation of breathing (in rabbits, rats, mice) or the induction into a surgical plane of anaesthesia (in dogs, the jawbone, pupil reflexes, paw relaxes, and tongue rigidity were continually monitored during the procedure), the chest was opened through a left thoracotomy. The heart was quickly excised from the chest. The detailed protocols for heart perfusion and single cell dispersion are described in Supplementary material online.

2.1.2 Patch clamp

Myocytes were patch-clamped using the whole-cell configuration in either current-clamp (for AP recording) or voltage (or AP)-clamp mode (for I_{to} or $I_{Ca,L}$ recording) as in our previous publications.[11,18–20] To record I_{to}, the $I_{Ca,L}$ blocker Cd^{3+} (0.3 mM) and Na current blocker TTX (10 μM) were added to Tyrode's solution. Cells were paced at a pacing cycle length (PCL) of 1 and 6 s to study the rate dependence of I_{to} and EADs. All experiments were carried out at 34–36°C.

2.1.3 Pacing protocols

A dynamic pacing protocol was used to measure APD restitution. The myocytes were paced at PCLs of 5, 2, 1 s, 700 ms for 6 beats each, and then at PCL 400 ms, decremented every 12 beats by 20 ms (from 400 to 300 ms), 10 ms (from 300 to 200 ms), or 5 ms (from 200 to 150 ms), or until a 2:1 block occurred. Recovery of I_{to} from the inactivation was investigated using a conventional two-pulse protocol: an inactivating pulse depolarizing to +40 mV for 400 ms (P_1) followed by a variable recovery interval (5, 10, 20, 50, 100, 300, 600 ms; 1, 3, 6, 10, 15 s, respectively) and subsequent +40 mV test pulse (P_2). The interpulse potential was set at − 80 mV.

2.2 Computer simulation and theoretical analysis

Simulations were carried out in single myocyte models with the following governing equation for voltage (V): $C_m dV/dt = -I_{ion} + I_{sti}$, where $C_m = 1\ \mu F/cm^2$, I_{ion} is the total ionic current density, and I_{sti} is the stimulation current density. I_{ion} formulation was taken from the rabbit ventricular myocyte AP model by Mahajan *et al.*[21] with modifications. Modifications to the model were made to better fit the APD restitution and EAD properties observed in the experimental studies. The major changes include substitution of $I_{Ca,L}$ by the Hodgkin-Huxley type of formulation as in the 1994 Luo and Rudy model (LR2)[22] and I_{to} by the formulation modified from the one by Dong *et al.*[23] Therefore, the ionic current density of the rabbit ventricular model became: $I_{ion} = I_{Na} + I_{to} + I_{Ca,L} + I_{Ks} + I_{Kr} + I_{NCX} + I_{K1} + I_{NaK}$. The effects of H_2O_2 on ion channels were modelled by increasing $I_{Ca,L}$, late I_{Na}, Na-Ca exchange current (I_{NCX}), and I_{to}, based on previous[11,13,14,17] and present experimental studies. 4-AP is known to inhibit different components of I_{to}.[24] For simplicity, however, we modelled the 4-AP effect by only reducing the maximum conductance of I_{to} with the goal of reducing 4-AP sensitive currents. Details of the modifications and formulations of the ionic currents are presented in Supplementary material online, Methods and *Figures S2–6*.

To study the general mechanism of I_{to} promoting EADs and for the convenience of theoretical analysis, we used the 1991 Luo and Rudy (LR1) model[25] and added an I_{to} to the LR1 model, with I_{to} modified also from the formulation by Dong *et al.*[23] (see Supplementary material online, Methods and *Figures S7–8*). The total ionic current density was $I_{ion} = I_{Na} + I_{Ca,L} + I_K + I_{K1} + I_{Kp} + I_b + I_{to}$. The rationale for choosing LR1 is because it is much simpler than the rabbit ventricular model and it has the minimum requirements for EADs to occur, as shown in the previous study.[10] Using this simple model, we can follow the same method as in the previous study[10] to perform bifurcation analysis to understand how I_{to} promotes EADs (see Supplementary material online, *Figure S11*).

3. Results

3.1 I_{to} promotes EADs in rabbit ventricular myocytes

EADs are usually promoted by bradycardia because during the longer diastolic intervals[26] the delayed rectifier K channels enter the states that are deeply closed, thus reducing outward currents and lengthening the APD. However, in rabbit ventricular myocytes, the APD first increases as the heart rate decreases, but then becomes shorter at very slow heart rates (i.e. the APD restitution curve is biphasic) (*Figure 1A* and *B*). This has been attributed to the slow recovery of I_{to} in the rabbit cells.[27] However, it is at these very slow heart rates (PCL $>$ 3 s) that exposure to H_2O_2 induces EADs, but not at the intermediate heart rates at which the APD is normally longer (*Figure 1C*).[11,19] We assessed the role of I_{to} in the EAD formation by applying 4-AP to block I_{to}. As shown in *Figure 1D* and *E*, 4-AP (2 mM) alone prolonged APD at all PCL, to a greater extent at the long PCL (e.g. 6 s), and to a less extent at short PCLs (e.g. 1 s). Therefore, the restitution curve was transformed from a biphasic shape to a monophasic one. Despite prolonging the APD at very slow heart rates, 4-AP paradoxically prevented overt EADs in response to 200 μM H_2O_2 (*Figure 1F*). The same phenomenon was observed in

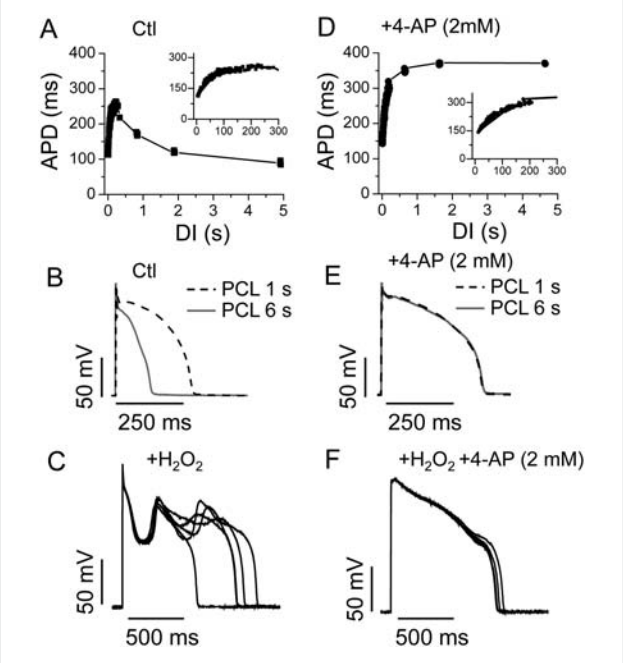

Figure 1 Dependence of APD and EAD genesis on I_{to}. (*A*) The APD restitution curve obtained from a rabbit ventricular myocyte showing a biphasic change of the APD. The expanded region between 0 and 300 ms is shown in the insets. DI, diastolic interval. (*B*) APs recorded at PCL 6 s (grey solid) and 1 s (dashed). (*C*) H_2O_2 (200 μM, perfusion for 6 min) induced EADs at PCL = 6 s. (*D*–*F*) Same as (*A*)–(*C*), but in the presence of 2 mM 4-AP. Note that 4-AP eliminated the EADs (*F*). Five consecutive APs are shown in panels (*C*) and (*F*).

20 cells from 8 rabbits. It should be noted that some cells from rabbits showed a less negative slope in the biphasic restitution curve, suggesting a lower I_{to} level. However, these cells exhibited similar responses to H_2O_2 for inducing EADs and to 4-AP for attenuating EADs (data not shown).

3.2 Effects of H_2O_2 on I_{to} kinetics and conductance

Under our experimental conditions, H_2O_2 enhanced I_{to} in a time course comparable with that for the EAD onset.[11] This was attenuated by 4-AP (*Figure 2A* and *B*). H_2O_2 increased both the peak amplitude of I_{to} and the magnitude of the current at the late phase under the 400 ms-pulse clamp (we refer to the late component as I_{late}, including the slow and non-inactivating components) (*Figure 2C*). Finally, H_2O_2 slowed the I_{to} inactivation by decreasing the time constants of both the slow ($\tau_{s,in}$) and fast components ($\tau_{f\ in}$) (*Figure 2D*).

Under control conditions and consistent with APD shortening at PCL $>$ 3 s, I_{to} displayed a slow recovery from inactivation, as shown in *Figure 2E* and *G*. I_{to} recovery from the inactivation was best fit with a double exponential equation (see Supplementary material online, Methods) where the averaged time constants for the fast ($\tau_{f,\ re}$) and slow ($\tau_{s,\ re}$) components are 832 $\pm$ 222 ms and 5.8 $\pm$ 2.1 s, respectively. H_2O_2 accelerated the recovery from the inactivation of I_{to}, mainly by decreasing $\tau_{f,\ re}$ to 240 $\pm$ 61 ms, while $\tau_{s,\ re}$ showed no significant change (*Figure 2F*–*H*). The amplitudes of the fast and slow components (A_f: 0.22 $\pm$ 0.08 and A_s: 0.79 $\pm$ 0.14 under control conditions) were significantly affected by H_2O_2, (A_f: 0.40 $\pm$ 0.05 and A_s: 0.61 $\pm$ 0.04) ($P < 0.05$, $n = 6$).

3.3 Effect of I_{to} on $I_{Ca,L}$ during the AP during H_2O_2 exposure

Since $I_{Ca,L}$ reactivation plays an essential role in EAD genesis, we compared the effects of an AP with or without I_{to} on $I_{Ca,L}$ during an AP clamp. When the cells were clamped with the AP morphology corresponding to the presence of I_{to} (i.e. an AP pre-recorded at a PCL 6 s), $I_{Ca,L}$ was significantly larger both in the absence and presence of H_2O_2, than those recorded during the AP morphology corresponding to the absence of I_{to} (i.e. rectangular AP pre-recorded at PCL 1 s) (see Supplementary material online, *Figure S1*). This result indicates that the presence of I_{to} lowers the AP plateau voltage into a voltage range that produces a larger inward $I_{Ca,L}$, known to be a key factor in EAD formation.[28,29]

3.4 I_{to} promotes EADs in an AP model of rabbit ventricular myocytes

To understand how I_{to} promotes EAD genesis, we carried out simulations using a rabbit ventricular AP model,[21] modified to include the property of slow recovery of I_{to} observed experimentally. The effects of H_2O_2 were modelled by increasing the late I_{Na}, $I_{Ca,L}$, and I_{to} (see Supplementary material online, Methods and *Figures S2*–*6*). The APD restitution curve for the control (*Figure 3A* and *B*) was biphasic, similar to experimental data. When the effects of H_2O_2 on ionic currents were simulated, EADs occurred only at slow pacing rates (*Figure 3C*). When we removed I_{to} from the model to simulate the effects of blocking I_{to} with 4-AP, the APD restitution curve became monotonic (*Figure 3D* and *E*), and no EADs were observed (*Figure 3F*). These data agree well with the experimental observations shown in *Figure 1*.

To show how I_{to} interacts with other currents to potentiate EADs, we plotted voltages along with I_{to}, $I_{Ca,L}$, I_{Ks}, and I_{NCX} under different conditions in *Figure 4*. In the control case (*Figure 4A* and *B*), I_{to} was larger during slower pacing (PCL 6 s) due to its slow recovery, which lowered the voltage at the plateau phase. This in turn caused a larger peak $I_{Ca,L}$, a larger I_{NCX}, and a very small I_{Ks}; however, the APD was shorter. When the effects of H_2O_2 were simulated (*Figure 4C* and *D*), the AP and the ionic currents at PCL = 1 s were similar to those of the control at PCL = 1 s. At PCL = 6 s (*Figure 4D*), EADs were induced by H_2O_2. In this case, a larger I_{to} resulted in a lower AP plateau voltage that caused a larger peak $I_{Ca,L}$ and a larger I_{NCX}. Concomitantly, the activation of I_{Ks} was much slower due to the lower AP plateau voltage (here the activation time constant of I_{Ks} vs. voltage is reproduced in Supplementary material online, *Figure S9*), which also played an important role in allowing the inward currents to reverse repolarization and cause EADs. When I_{to} was partially blocked (*Figure 4E*), the AP plateau voltage was elevated, resulting in a smaller peak $I_{Ca,L}$, a smaller I_{NCX}, and a much larger I_{Ks}, which prevented EADs from forming.

3.5 Mechanisms by which I_{to} promotes EADs

As shown in *Figure 4*, I_{to} did not directly cause EADs; rather, its effects on voltage caused complex changes in other currents, making it difficult to sort out the general underlying mechanism. To simplify the analysis, we used the LR1 model with modifications to reduce

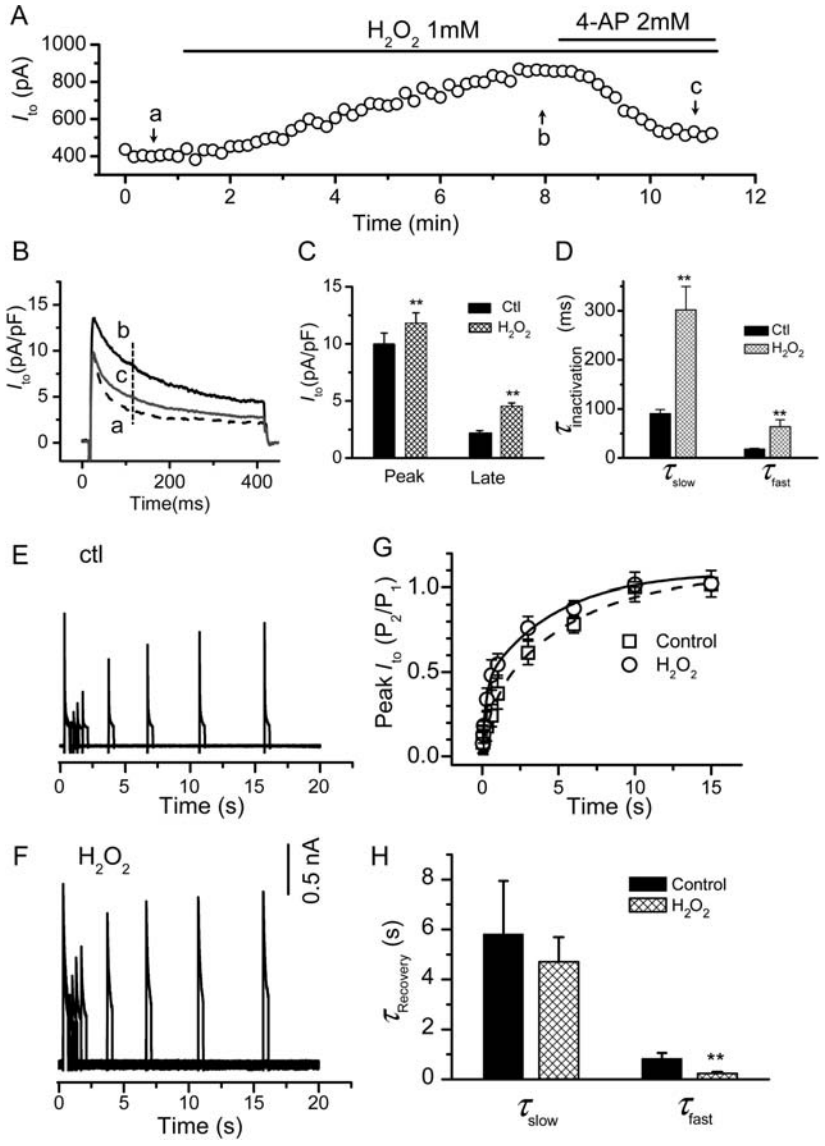

Figure 2 Effect of H_2O_2 I_{to} in rabbit ventricular myocytes. (*A–D*) Effects of H_2O_2 on I_{to} amplitude and inactivation: I_{to} was elicited by depolarization to + 60 mV from a holding potential of −70 mV every 10 s. (*A*) The time course showing the effect of H_2O_2 and 4-AP on the I_{to} amplitude. The current values measured at 100 ms after the depolarization pulse [as indicated by the dashed line in (*B*)]. The current traces at point a, b, c are shown in (*B*). (*C*) Bar graph summarizing the effect of H_2O_2 on peak and late currents (measured at the end of 400 -ms pulse). (*D*) H_2O_2 slowed down the inactivation of both the fast and slow components of I_{to}. $^{**}P < 0.01$ compared with control ($n = 7$). (*E–H*) Effect of H_2O_2 on the recovery from inactivation: (*E*) representative I_{to} traces following a standard two-pulse protocol (supplements) to measure the recovery from inactivation under control in the absence of H_2O_2 (Ctl). P_2/P_1 is the ratio of the test pulse current/inactivating pulse current amplitudes. The inactivated current amplitude was measured by the difference between the peak inactivating pulse current or the test pulse current and the current at the end of the inactivating pulse. The inter-pulse potential was set at −80 mV. (*F*) The same as (*E*), in the presence of 1 mM H_2O_2. (*G*) Summarized peak I_{to} values fitted to a two-term exponential function. (*H*) The effect of H_2O_2 on time constants for slow (τ_{slow}) and fast (τ_{fast}) components.

repolarization reserve (see Supplementary material online for detailed changes). Under this (control) condition, the APD is long with no EAD presence (*Figure 5A*). Consistent with the results from myocyte experiments and the rabbit ventricular AP model, adding an I_{to} to the control AP induced EADs (*Figure 5B*). In this case, $I_{Ca,L}$ was increased and the activation of the time-dependent K current (I_K, similar to I_{Ks} in the rabbit ventricular AP model) was slowed due to the lowering of the plateau voltage, similar to the more detailed rabbit ventricular AP model. When I_{to} was increased to a higher value, the APD became very short and no EADs could form (*Figure 5C*).

In *Figure 5D* and *E*, we scanned the parameters of I_{to} conductance (G_{to}) and its inactivation time constant for EADs and the APD, respectively. EADs only occurred in the intermediate ranges of conductance and the inactivation time constant, whereas small or large conductance and slow or fast inactivation suppressed EADs. When I_{to} inactivation was fast, an increase in I_{to} conductance first increased the APD (and EADs) but then caused a sudden transition to a short

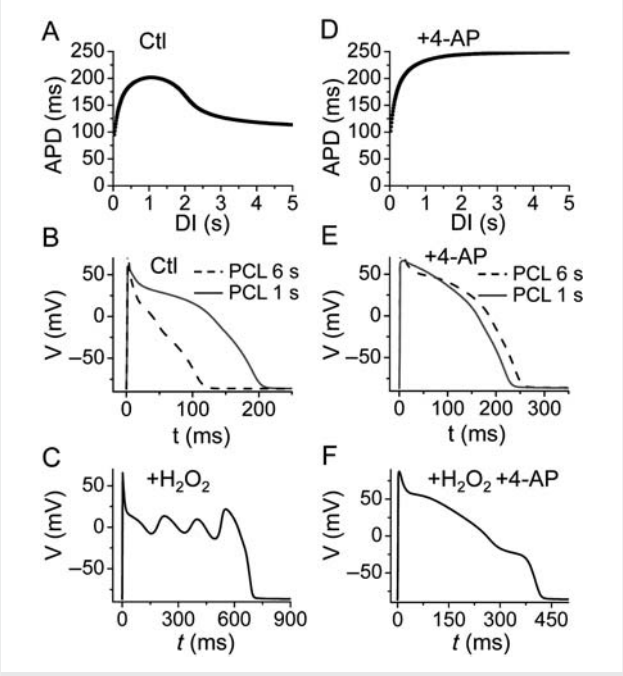

Figure 3 APD restitution and H_2O_2-induced EADs in the rabbit ventricular model in the presence of I_{to}. The plots are an analogy to *Figure 1*. (*A*) The APD restitution curve of the control cases. (*B*) Control APs for PCLs of 6 s (grey solid) and 1 s (dashed). (*C*) Simulated H_2O_2-induced EADs. (*D*–*F*) The same as (*A*)–(*C*), but in the presence of 4-AP and I_{to} blocked.

APD when the I_{to} conductance was greater than a critical value (colour changes from green or red to blue suddenly in *Figure 5E*). When I_{to} inactivation was slow, the APD decreased continuously as the I_{to} conductance increased. These effects of I_{to} on the APD agree with those observed in previous studies.[23,30] In fact, a very slow-inactivating I_{to} component suppresses EADs (see Supplementary material online, *Figure S10*).

To further understand how I_{to} promotes EADs, we used non-linear dynamics and bifurcation theory following the method in a previous study by Tran *et al.*[10] Details of this analysis and discussion are presented in Supplementary material online (Section 2.3 and *Figure S11*). The major finding is that I_{to}, with a proper conductance and inactivation speed, can bring the membrane voltage into the window to undergo the bifurcation that is required for voltage oscillations and thus EADs.

3.6 The role of I_{to} in EAD formation in cardiac cells of other species

It is well known that the molecular composition, current density, and kinetics (e.g. inactivation and recovery from inactivation) of I_{to} vary in different species and locations in the heart. To validate the general predictions from the general theoretical analysis (*Figure 5D–E*), we carried out additional experiments in ventricular cells from rats, mice, and canine epicardium, as well as canine Purkinje cells. Experimental results are shown in detail in Supplementary material online, *Figures S12–15* and summarized and compared qualitatively with simulations in *Figure 6*.

Since we showed that H_2O_2 increases both $I_{Ca,L}$ and I_{to} and in order to compare with experimental results, we first scanned the I_{to} conductance and $I_{Ca,L}$ conductance on EAD formation in the LR1 model for slow and fast I_{to} inactivation (*Figure 6A* and *D*). *Figure 6A* was obtained for an I_{to} inactivation time constant in the intermediate range as shown in *Figure 5D*. In our model, EADs occurred in large $I_{Ca,L}$ conductance and intermediate I_{to} conductance (grey region). For rabbit (*Figure 6Ba* and *C*) and rat ventricular myocytes (*Figure 6Bb*), H_2O_2 increased $I_{Ca,L}$ and I_{to}, caused the AP to exhibit EADs. Blocking I_{to} by 4-AP (at either a low or high concentration) eliminated EADs. This is illustrated in *Figure 6A* by the transition from the black open circle (no EAD region) to the red closed circle (EAD region) and then to the blue open circle (no EAD region). For mouse ventricular myocytes (*Figure 6Bc*) and canine Purkinje cells (*Figure 6Bd* and *C*); however, H_2O_2 did not promote EADs. But partially blocking I_{to} by a low dose of 4-AP (50–100 μM) promoted EADs, which were eliminated by a higher dose of 4-AP (2 mM). This indicates that either I_{to} was already high in the control and/or H_2O_2 activated too much additional I_{to}. This scenario is illustrated in *Figure 6A* by the transitions from black open triangle (no EAD region) to the open red triangle (no EAD region), then to the red closed circle (EAD region), and finally to the blue open circle (no EAD region). In canine epicardial myocytes, the inactivation of I_{to} is very fast (~19.9 ms). Based on our theoretical analysis, the propensity for EADs is greatly reduced for fast I_{to} inactivation (*Figures 5D* and *6D*), and indeed we were not able to induced EADs in canine ventricular myocytes by H_2O_2 (*Figure 6E*). This is illustrated by the transitions of *Figure 6*D. In summary, the experimental results agree qualitatively well with the theoretical predictions for all the species and cell types analysed. Thus I_{to} with a proper conductance and inactivation time constant can promote EADs in cardiac myocytes, independent of species.

4. Discussion

I_{to} has been shown to play important roles in AP morphology and APD alternans.[1–3] In this study, we carried out both experiments and simulations to study the effects of I_{to} on EAD genesis in cardiac cells exposed to H_2O_2. In rabbit ventricular myocytes, EADs occurred only at slow pacing rates and were eliminated by either shortening PCL or blocking I_{to} with 4-AP. The experimental observations were confirmed in computer simulations of an AP model of rabbit ventricular myocytes. We have shown in general that I_{to} with a proper conductance and inactivation time constant can bring membrane voltage into the window allowing $I_{Ca,L}$ reactivation before I_{Ks} is fully activated to repolarize the myocytes. In addition, this lowering of the AP plateau also brings I_{Ks} into a voltage range where its activation is the slowest, further decreasing the repolarization reserve. These two effects together potentiate voltage oscillations and thus EAD generation. When I_{to} is weak or inactivates too quickly, the AP is long but no EADs can be induced. When I_{to} is too strong or inactivates too slowly, the AP is short and no EADs occur either. This general prediction of the effects of I_{to} on EAD genesis was validated in cardiac cells isolated from other species.

4.1 Reduced repolarization reserve and EAD genesis

The repolarization reserve is a concept articulated originally by Roden[31] stating that normal ventricles have a redundancy in total repolarizing currents (mainly K currents), ensuring rapid repolarization. However, when this reserve is reduced, the cell loses the ability of normal repolarization and exhibits an excessive prolongation of APD. Based on the dynamical analysis by Tran *et al.*[10] and the present study (see

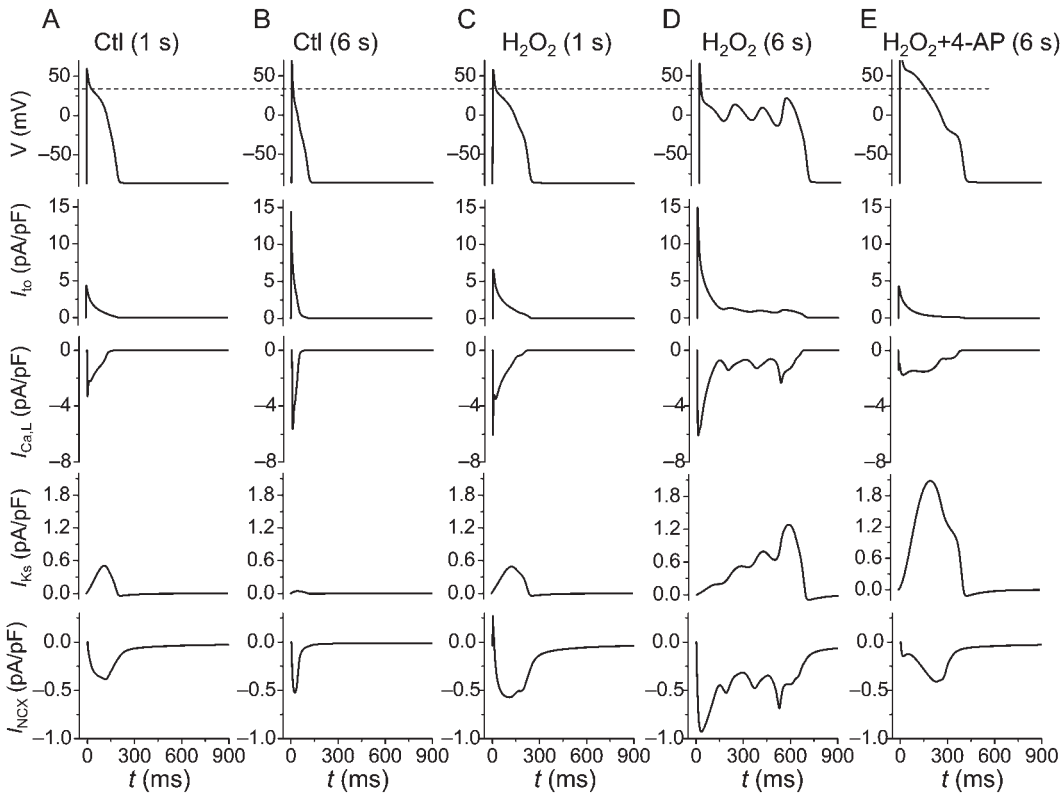

Figure 4 I_{to}-induced ionic current changes in the rabbit ventricular model. AP, I_{to}, $I_{Ca,L}$, I_{Ks}, and I_{NCX} were plotted under different conditions. The dashed line in the top row indicates the plateau level of AP under the control condition. (*A* and *B*) The cell was paced at PCLs of 1 and 6 s, respectively, in the absence of H_2O_2. (*C* and *D*) The cell was paced at PCLs of 1 and 6 s, respectively, in the presence of H_2O_2. Note that EADs were induced by H_2O_2 at PCL 6 s. (*E*) H_2O_2-induced EADs were eliminated by partially blocking I_{to}.

Supplementary material online, *Figure S11*), we show that membrane voltage needs to decrease 'fast' enough to enter an oscillatory window before slowly activating repolarization currents, such as I_{Ks}, grow too large. In the study by Tran *et al.*,[10] EADs were induced by increasing the maximum conductance of $I_{Ca,L}$ and slowing the activation of the time-dependent K current to reduce repolarization reserve. In the present study, we did not slow the activation of the repolarizing currents directly, but rather added I_{to}, which accelerated the early repolarization phase of the AP, bringing the voltage to the window range to undergo the bifurcation to promote EADs. However, it should be noted that when I_{to} becomes very large (such as would occur with a specific I_{to} activator), it causes sufficient AP shortening to suppress EAD formation. Therefore, strong repolarization (enhanced repolarization reserve) is needed to bring the voltage into the window for $I_{Ca,L}$ reactivation, but once the voltage is in this window, weak repolarization (reduced repolarization reserve) is needed to maintain the voltage at this window for oscillations and thus EADs. Notably a recent study has shown that coupling to fibroblasts can also speed up the early repolarization phase of a myocyte AP and promote EAD generation.[32]

4.2 Roles of different I_{to} components in EAD genesis

At least two major I_{to} components, i.e. fast ($I_{to,f}$) and slow ($I_{to,s}$) components are present in adult myocytes.[33] It has been suggested that pore-forming α subunits for Kv4.2 and Kv4.3 encode $I_{to,f}$, whereas Kv1.4 encodes $I_{to,s}$. They differ in the kinetics of inactivation and, in particular, the kinetics of recovery from inactivation. $I_{to,f}$ recovers very rapidly with time constants in the range from tens to hundreds of milliseconds, while $I_{to,s}$ recovers slowly with time constants in the range of seconds.[34]

The I_{to} components and their density are different in different species as well as different regions in the same heart. The kinetic properties of I_{to} in rabbit ventricular myocytes are substantially different from those of canine/human ventricular myocytes. The rabbit ventricular I_{to} is at least 10 times slower to inactivate and recover from inactivation than canine/human ventricular I_{to}.[34] The epicardial myocytes from a canine left ventricle only express the high level of $I_{to,f}$.[35] In contrast, both $I_{to,f}$ and $I_{to,s}$ are present in canine and human Purkinje cells.[36–39]

Different components of I_{to} have different effects on AP properties. For example, in canine ventricular cells that only have the fast component, the presence of a moderate I_{to} prolongs AP, whereas a high I_{to} substantially shortens AP, resulting in a sudden discontinuous change in the APD as I_{to} increases.[40] In rabbit myocyte and canine Purkinje cells, I_{to} inactivates slowly with a non-inactivating steady-state component,[38] whose presence always shortens the AP. This was demonstrated in *Figure 1* in which the rabbit APD was shortened as the pacing rate decreased due to the slow recovery ($\tau_{slow,\ re} = 5.8 \pm 2.1$ s) of I_{to}. The 4-AP-induced APD prolongation (*Figure 1E* and *F*) was at least partially due to the blockage of this non-inactivating component.

As to the roles of the multiple components of I_{to} in EAD genesis, we showed that EADs only occurred in a certain range of I_{to} conductance and inactivation speed (*Figure 5*). In fact, a very slow-inactivating

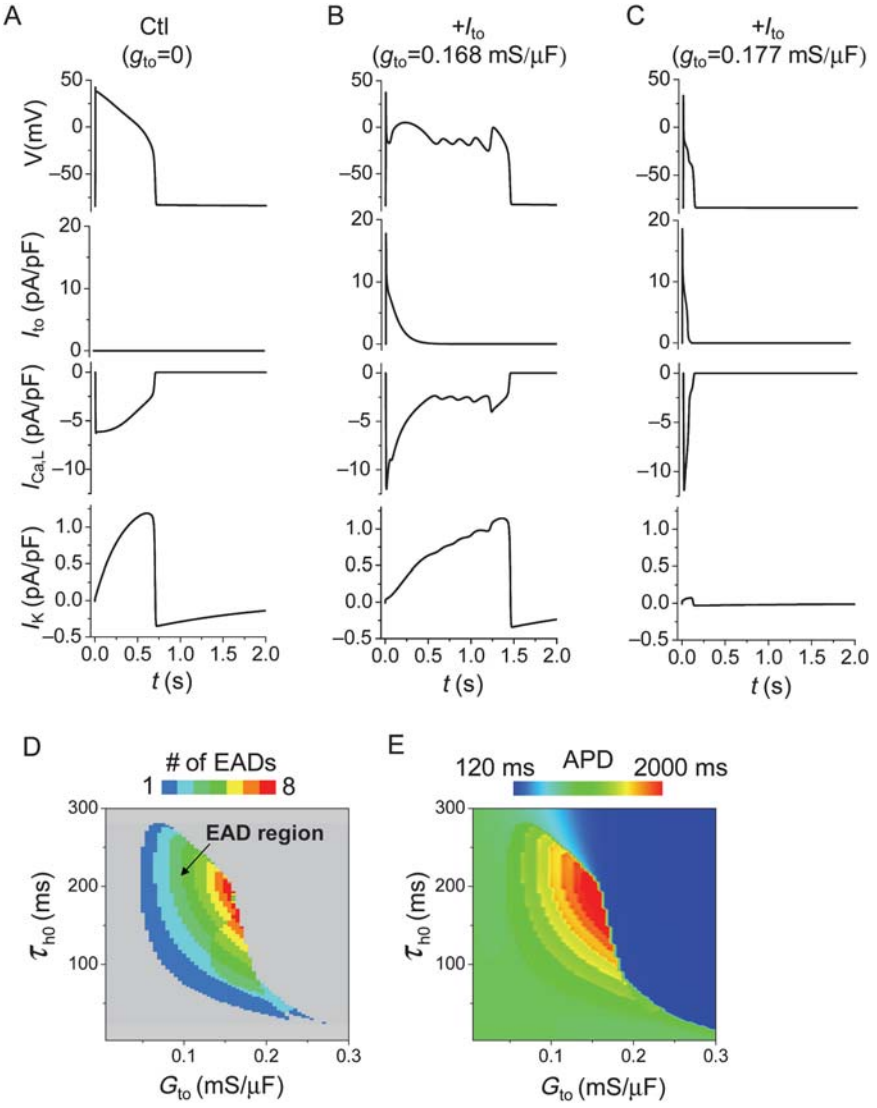

Figure 5 Effects of I_{to} on EAD genesis in the LR1 model. APs, I_{to}, $I_{Ca,L}$, and I_K were plotted for three different conditions. (*A*) Control, no I_{to}. (*B*) A proper I_{to} added to the control model induced EADs. (*C*) A larger I_{to} shortened the APD and eliminated EADs. (*D*) Phase diagram showing the EAD region (coloured) in the I_{to} conductance (G_{to}) and τ_{h0} parameter space. τ_{h0} is the constant component of the inactivation time constant τ_h of I_{to}, i.e. $\tau_h = \tau_{h0} + \tau_h(V)$ [see equation (17) in the Supplementary material online, Methods]. (*E*) The APD distribution in the I_{to} conductance and the τ_{h0} parameter space.

I_{to} component suppresses EADs (see Supplementary material online, *Figure S10*). This may also explain why a moderate decrease in I_{to} density results in the elevation of the AP plateau and the enhancement of EADs in mouse myocytes and canine Purkinje cells (*Figure 6* and see Supplementary material online, *Figures S13 and 14*). On the other hand, if the I_{to} inactivation is too fast, such as in canine ventricular myocytes, it is not sufficient to promote EADs and is cardioprotective.

4.3 Role of H_2O_2 in EAD genesis

It has been shown that H_2O_2 activates late I_{Na} and increases $I_{Ca,L}$; both are considered to be the major ionic mechanisms for a H_2O_2-induced EAD.[11,13–15] Here, we show that H_2O_2 also enhances the conductance of I_{to}, slows its inactivation, and accelerates its recovery from inactivation. This resembles the effect of CaMKII on the mammalian A-type K^+ channel $K_V1.4$.[41] The findings of the present study indicate that H_2O_2-mediated activation of I_{to} also plays an important role in EAD genesis. Han *et al.*[36] showed that H_2O_2 only activated I_{to} in canine Purkinje cells, but not in ventricular myocytes. This explains why H_2O_2 first caused further suppression of the low plateau in Purkinje cells before EAD generation. H_2O_2 only generated a dome in canine ventricular myocytes presumably by purely reactivation of $I_{Ca,L}$.

While more direct evidence is needed to validate the involvement of ROS in EAD genesis *in vivo*, a growing body of evidence has comprehensively established the link between an elevated ROS level and

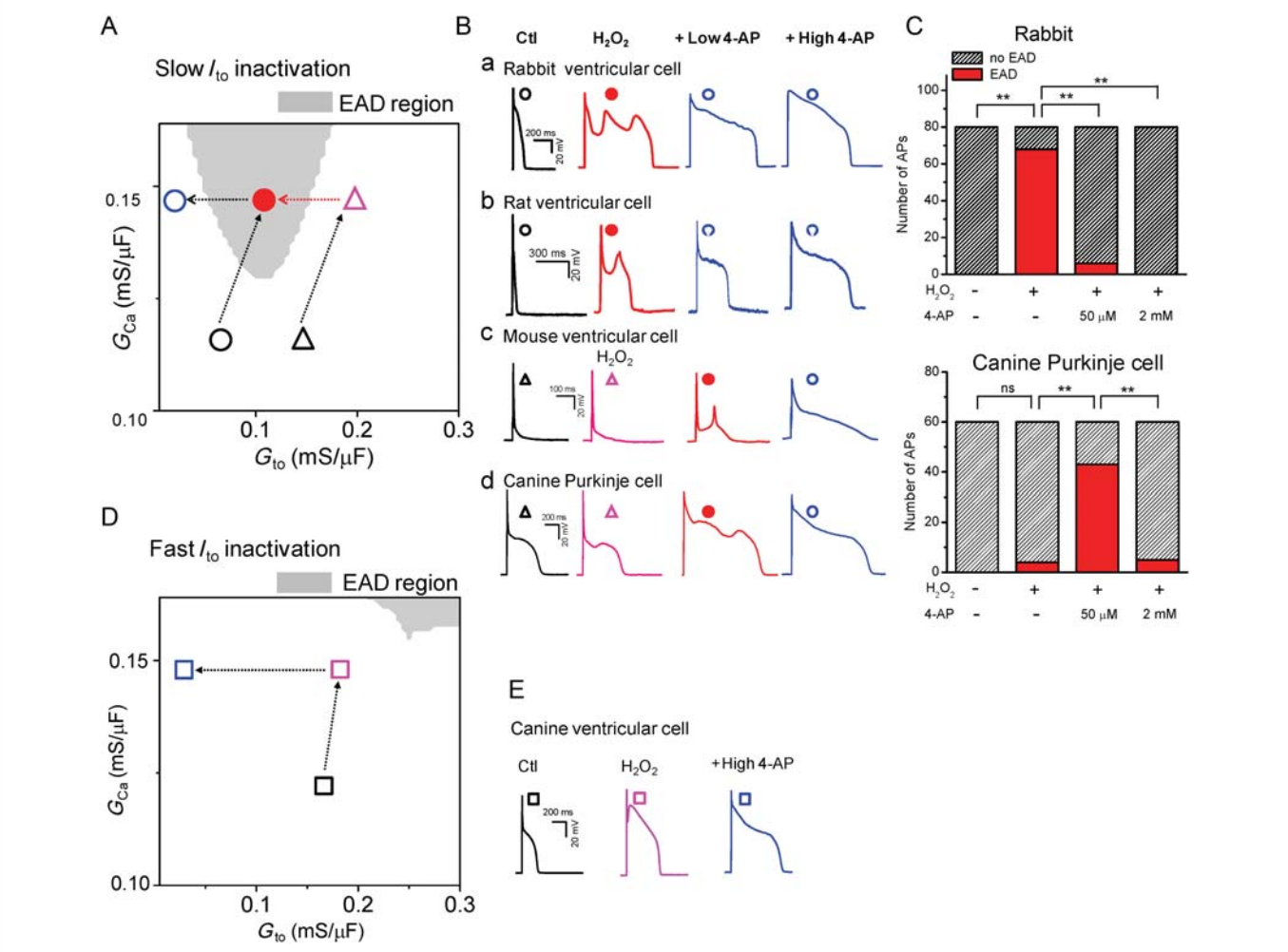

Figure 6 Roles of I_{to} in EAD genesis in different species. (*A*) The EAD distribution in the $I_{Ca,L}$ and I_{to} conductance (G_{Ca} and G_{to}) space, using the same model as in *Figure 5*. The inactivation time constant of the I_{to} is the intermediate value (τ_{h0}= 200 ms) as revealed by *Figure 5D*. The EAD occurrence region is marked in grey. (*B*) APs recorded in different species as indicated (a–d). The black and coloured symbols mark the putative locations of the APs in the distribution diagram (*A*). (*C*) Summarized bar graphs showing the incidence of EADs within 20 APs ($n \geq 3$ cells). ns, not significant; $^{**}P < 0.01$ by Fisher's exact test. (*D*) The same as (*A*), except that the inactivation time constant of the I_{to} is fast (τ_{h0}= 20 ms), which is similar to that of canine ventricular myocytes. (*E*). APs recorded from canine ventricular myocytes. The symbols mark the putative locations of the APs in the distribution diagram (*C*).

high propensity for cardiac arrhythmias in a number of circumstances, such as coronary heart disease, heart failure, and ageing.[42–46] Moreover, a recent whole-heart study has shown that H_2O_2 causes EADs and focal ventricular arrhythmias in the aged fibrotic hearts.[47]

4.4 Limitations

It should be noted that in either experiments or simulations, I_{to}, an outward current *per se* cannot induce EADs. Other conditions (such as applying H_2O_2 in the experiments to activate inward currents, i.e. I_{Na} and $I_{Ca,L}$) must be satisfied. In addition, the mechanisms by which I_{to} contributes to EADs may be more complicated than those revealed in the simple model. For example, lowering the AP plateau promotes the Ca influx into the cell due to the reactivation of $I_{Ca,L}$, elevating intracellular Ca concentration and thus I_{NCX}, which could be the primary factor potentiating EADs. The elevation of Ca concentration may also affect CaMKII signalling, which affects many targets (such as $I_{Ca,L}$, late I_{Na}, and RyR).[11,14,48] In fact, the prolonged treatment by H_2O_2 occasionally induced both DADs and EADs, or even sustained the depolarization of the membrane potential, most likely due to intracellular Ca overload.[11] In a recent study[49] we have demonstrated that the ionic mechanisms for EAD generation can be dominated by either $I_{Ca,L}$ reactivation or spontaneous Ca release (Ca waves)-induced increase of I_{NCX} in different models. This study focuses on EADs primarily caused by the reactivation of $I_{Ca,L}$. We would expect that I_{to} would play a less important role in Ca wave-induced DADs or EADs.

Nevertheless, by a combination of experiments and simulations, we show here that the presence of I_{to} plays an important role in EAD genesis under the condition of reduced repolarization reserve. This may provide useful insights into the development of novel therapeutic strategies for EAD-related arrhythmias. Our results suggest that, in general, blocking I_{to} helps to prevent EADs under the condition of reduced repolarization reserve, such as the clinical settings of the long QT syndrome and heart failure. However, it should be noted

that complex changes (remodelling) occur in heart failure and many changes in Ca cycling are arrhythmogenic.

Supplementary material

Supplementary material is available at *Cardiovascular Research* online.

Acknowledgements

The authors wish to thank Dr James N. Weiss for critical reading of the manuscript and his continuous support and encouragement.

Conflict of interest: none declared.

Funding

This study is supported by a Postdoctoral Fellowship from American Heart Association Western states affiliate (Y.X.), HL 66140 (P.A.B.), NIH/NHLBI P01 HL078931 and the Laubisch endowments (Z.Q.), and NIH/NHLBI R01 HL97979 (L.H.X.).

References

1. Maoz A, Krogh-Madsen T, Christini DJ. Instability in action potential morphology underlies phase 2 reentry: a mathematical modeling study. *Heart Rhythm* 2009;**6**:813–822.
2. Qu Z, Xie Y, Garfinkel A, Weiss JN. T-wave alternans and arrhythmogenesis in cardiac diseases. *Frontiers Physiol* 2010;**1**:154.
3. Lukas A, Antzelevitch C. Phase 2 reentry as a mechanism of initiation of circus movement reentry in canine epicardium exposed to simulated ischemia. *Cardiovasc Res* 1996;**32**:593–603.
4. Antzelevitch C, Nof E. Brugada syndrome: recent advances and controversies. *Curr Cardiol Rep* 2008;**10**:376–383.
5. Guo W, Li H, London B, Nerbonne JM. Functional consequences of elimination of $I_{to,f}$ and $I_{to,s}$: early afterdepolarizations, atrioventricular block, and ventricular arrhythmias in mice lacking Kv1.4 and expressing a dominant-negative Kv4 α subunit. *Circ Res* 2000;**87**:73–79.
6. Antzelevitch C. Ionic, molecular, and cellular bases of QT-interval prolongation and torsade de pointes. *Europace* 2007;**9**(Suppl 4):iv4–15.
7. Moss AJ, Kass RS. Long QT syndrome: from channels to cardiac arrhythmias. *J Clin Invest* 2005;**115**:2018–2024.
8. Biliczki P, Virag L, Iost N, Papp JG, Varro A. Interaction of different potassium channels in cardiac repolarization in dog ventricular preparations: role of repolarization reserve. *Br J Pharmacol* 2002;**137**:361–368.
9. Roden DM. Long QT syndrome: reduced repolarization reserve and the genetic link. *J Intern Med* 2006;**259**:59–69.
10. Tran DX, Sato D, Yochelis A, Weiss JN, Garfinkel A, Qu Z. Bifurcation and chaos in a model of cardiac early afterdepolarizations. *Phys Rev Lett* 2009;**102**:258103.
11. Xie LH, Chen F, Karagueuzian HS, Weiss JN. Oxidative-stress-induced afterdepolarizations and calmodulin kinase II signaling. *Circ Res* 2009;**104**:79–86.
12. Erickson JR, Joiner ML, Guan X, Kutschke W, Yang J, Oddis CV *et al*. A dynamic pathway for calcium-independent activation of CaMKII by methionine oxidation. *Cell* 2008;**133**:462–474.
13. Song YH, Cho H, Ryu SY, Yoon JY, Park SH, Noh CI *et al*. L-type Ca^{2+} channel facilitation mediated by H_2O_2-induced activation of CaMKII in rat ventricular myocytes. *J Mol Cell Cardiol* 2010;**48**:773–780.
14. Ward CA, Giles WR. Ionic mechanism of the effects of hydrogen peroxide in rat ventricular myocytes. *J Physiol* 1997;**500**(Pt 3):631–642.
15. Song Y, Shryock JC, Wagner S, Maier LS, Belardinelli L. Blocking late sodium current reduces hydrogen peroxide-induced arrhythmogenic activity and contractile dysfunction. *J Pharmacol Exp Ther* 2006;**318**:214–222.
16. Wagner S, Ruff HM, Weber SL, Bellmann S, Sowa T, Schulte T *et al*. Reactive oxygen species-activated Ca/calmodulin kinase IIdelta is required for late I_{Na} augmentation leading to cellular Na and Ca overload. *Circ Res* 2011;**108**:555–565.
17. Goldhaber JI, Parker JM, Weiss JN. Mechanisms of excitation-contraction coupling failure during metabolic inhibition in guinea-pig ventricular myocytes. *J Physiol(Lond)* 1991;**443**:371–386.
18. Goldhaber JI, Xie LH, Duong T, Motter C, Khuu K, Weiss JN. Action potential duration restitution and alternans in rabbit ventricular myocytes: the key role of intracellular calcium cycling. *Circ Res* 2005;**96**:459–466.
19. Sato D, Xie LH, Sovari AA, Tran DX, Morita N, Xie F *et al*. Synchronization of chaotic early afterdepolarizations in the genesis of cardiac arrhythmias. *Proc Natl Acad Sci USA* 2009;**106**:2983–2988.
20. Xie LH, Weiss JN. Arrhythmogenic consequences of intracellular calcium waves. *Am J Physiol Heart Circ Physiol* 2009;**297**:H997–H1002.
21. Mahajan A, Shiferaw Y, Sato D, Baher A, Olcese R, Xie LH *et al*. A rabbit ventricular action potential model replicating cardiac dynamics at rapid heart rates. *Biophys J* 2008;**94**:392–410.
22. Luo CH, Rudy Y. A dynamic model of the cardiac ventricular action potential. I. Simulations of ionic currents and concentration changes. *Circ Res* 1994;**74**:1071–1096.
23. Dong M, Sun X, Prinz AA, Wang HS. Effect of simulated I_{to} on guinea pig and canine ventricular action potential morphology. *Am J Physiol Heart Circ Physiol* 2006;**291**:H631–H637.
24. Brouillette J, Clark RB, Giles WR, Fiset C. Functional properties of K^+ currents in adult mouse ventricular myocytes. *J Physiol* 2004;**559**:777–798.
25. Luo CH, Rudy Y. A model of the ventricular cardiac action potential. Depolarization, repolarization, and their interaction. *Circ Res* 1991;**68**:1501–1526.
26. Silva J, Rudy Y. Subunit interaction determines I_{Ks} participation in cardiac repolarization and repolarization reserve. *Circulation* 2005;**112**:1384–1391.
27. Bassani RA, Altamirano J, Puglisi JL, Bers DM. Action potential duration determines sarcoplasmic reticulum Ca^{2+} reloading in mammalian ventricular myocytes. *J Physiol* 2004;**559**:593–609.
28. January CT, Riddle JM. Early afterdepolarizations: mechanism of induction and block. A role for L-type Ca^{2+} current. *Circ Res* 1989;**64**:977–990.
29. Tanskanen AJ, Greenstein JL, O'Rourke B, Winslow RL. The role of stochastic and modal gating of cardiac L-type Ca^{2+} channels on early after-depolarizations. *Biophys J* 2005;**88**:85–95.
30. Greenstein JL, Wu R, Po S, Tomaselli GF, Winslow RL. Role of the calcium-independent transient outward current I_{to1} in shaping action potential morphology and duration. *Circ Res* 2000;**87**:1026–1033.
31. Roden DM. Taking the 'idio' out of 'idiosyncratic': predicting torsades de pointes. *Pacing Clin Electrophysiol* 1998;**21**:1029–1034.
32. Nguyen TP, Xie Y, Garfinkel A, Qu Z, Weiss JN. Arrhythmogenic consequences of myofibroblast-myocyte coupling. *Cardiovasc Res* 2012;**93**:242–251.
33. Nerbonne JM. Molecular basis of functional voltage-gated K+ channel diversity in the mammalian myocardium. *J Physiol* 2000;**525**(Pt 2):285–298.
34. Patel SP, Campbell DL. Transient outward potassium current, I_{to}, phenotypes in the mammalian left ventricle: underlying molecular, cellular and biophysical mechanisms. *J Physiol* 2005;**569**:7–39.
35. Liu DW, Gintant GA, Antzelevitch C. Ionic bases for electrophysiological distinctions among epicardial, midmyocardial, and endocardial myocytes from the free wall of the canine left ventricle. *Circ Res* 1993;**72**:671–687.
36. Han W, Wang Z, Nattel S. A comparison of transient outward currents in canine cardiac Purkinje cells and ventricular myocytes. *Am J Physiol Heart Circ Physiol* 2000;**279**:H466–H474.
37. Han W, Zhang L, Schram G, Nattel S. Properties of potassium currents in Purkinje cells of failing human hearts. *Am J Physiol Heart Circ Physiol* 2002;**283**:H2495–H2503.
38. Jeck C, Pinto J, Boyden P. Transient outward currents in subendocardial Purkinje myocytes surviving in the infarcted heart. *Circulation* 1995;**92**:465–473.
39. Dun W, Boyden PA. The Purkinje cell; 2008 style. *J Mol Cell Cardiol* 2008;**45**:617–624.
40. Sun X, Wang HS. Role of the transient outward current I_{to} in shaping canine ventricular action potential-a dynamic clamp study. *J Physiol* 2005;**564**:411–419.
41. Roeper J, Lorra C, Pongs O. Frequency-dependent inactivation of mammalian A-type K^+ channel $K_V1.4$ regulated by Ca^{2+}/calmodulin-dependent protein kinase. *J Neurosci* 1997;**17**:3379–3391.
42. Lakatta EG, Sollott SJ. The 'heartbreak' of older age. *Mol Interv* 2002;**2**:431–446.
43. Slezak J, Tribulova N, Pristacova J, Uhrik B, Thomas T, Khaper N *et al*. Hydrogen peroxide changes in ischemic and reperfused heart. Cytochemistry and biochemical and X-ray microanalysis. *Am J Pathol* 1995;**147**:772–781.
44. Dhalla NS, Duhamel TA. The paradoxes of reperfusion in the ischemic heart. *Heart Metab* 2007;**37**:31–34.
45. Xing D, Chaudhary AK, Miller FJ Jr, Martins JB. Free radical scavenger specifically prevents ischemic focal ventricular tachycardia. *Heart Rhythm* 2009;**6**:530–536.
46. Tomaselli GF, Barth AS. Sudden cardio arrest: oxidative stress irritates the heart. *Nat Med* 2010;**16**:648–649.
47. Morita N, Sovari AA, Xie Y, Fishbein MC, Mandel WJ, Garfinkel A *et al*. Increased susceptibility of aged hearts to ventricular fibrillation during oxidative stress. *Am J Physiol Heart Circ Physiol* 2009;**297**:H1594–H1605.
48. Hashambhoy YL, Greenstein JL, Winslow RL. Role of CaMKII in RyR leak, EC coupling and action potential duration: a computational model. *J Mol Cell Cardiol* 2010;**49**:617–624.
49. Zhao Z, Wen H, Fefelova N, Allen C, Baba A, Matsuda T *et al*. Revisiting the ionic mechanisms of early afterdepolarizations in cardiomyocytes: predominant by Ca waves or Ca currents? *Am J Physiol Heart Circ Physiol* 2012;**302**:H1636–H1644.